Schottky barrier formation at the Fe/$SrTiO_3$(001) interface: Influence of oxygen vacancies and layer oxidation

R. Arras* and J. Gosteau
CEMES, Université de Toulouse, CNRS, UPS, 29 rue Jeanne Marvig, F-31055, Toulouse, France

S. Tricot and P. Schieffer
Université de Rennes 1, CNRS, IPR (Institut de Physique de Rennes)–UMR 6251, F-35000 Rennes, France

(Received 22 September 2020; accepted 12 November 2020; published 30 November 2020)

Schottky barrier formation at metal/insulating oxide interfaces relies on complex mechanisms which are difficult to unravel. We propose a detailed numerical study of the atomic, magnetic, and electronic properties of the Fe/$SrTiO_3$(001) interface, in which we focused our discussion on different parameters which can affect the Schottky barrier height (SBH). The interface termination appears to be the most critical aspect to be controlled for this interface: While an ideal TiO_2-terminated interface would guarantee a *n*-type barrier of about 1.2–1.6 eV, the presence of a SrO termination can drastically decrease its value down to few meV. The oxidation state of the interface is also an important criterium to maintain a high barrier value. Oxygen vacancies are always cited as the source of a deterioration of the SBH. For a TiO_2-terminated interface, we found that in their most stable position, i.e., in the interface layer, the oxygen vacancies do not affect the value of the SBH; when moving some atomic layers away from the interface, the SBH on the contrary decreases regularly. We propose that oxidizing the interface would allow us to improve the *n*-type SBH by healing the oxygen vacancies and forming an interfacial FeO layer, which seems favorable to the formation of a higher SBH.

DOI: 10.1103/PhysRevB.102.205307

I. INTRODUCTION

The association of a metal and an insulator or semiconductor is at the heart of the formation of capacitors and Schottky diode, and then at the basis of many derived electronic devices such as dynamic random access memories (DRAM) or metal-oxide-semiconductor field-effect transistors (MOSFET) [1,2]. A thorough study and understanding of their interface properties, and in particular of the interface oxidation state [3–6], is thus crucial to use these heterostructures in more and more performant and demanding applications.

$SrTiO_3$ (STO) is a common oxide substrate with a cubic perovskite structure at room temperature, a lattice parameter of 3.905 Å and an experimental band gap of 3.2 eV. This material is ideal to perform the epitaxial growth of several kinds of multifunctional oxides having the same perovskite structure, but also of metallic compounds. The use of insulating oxides such as STO is particularly interesting for many devices because of its high electric permittivity. Providing good control of its interface and a good choice of the metal, this oxide could allow us to get Schottky barrier heights enabling us to diminish the current leakage in miniaturized compounds. Among the main parameters to be controlled to optimize the interface properties, structural defects and in particular the oxygen vacancies (V_O's) are of the utmost importance [7–9]; they can especially participate to mechanisms turning the interface or some domains in the crystal to become metallic. For example, for more than 15 years now, STO has attracted lots of interest because of its ability to host a two-dimensional electron gas at its surface or interfaces [10–12]. If the origin of the two-dimensional electron gas is still debated, depending on the growth condition and on possible post treatments,V_O's can play a crucial role in its emergence and its conduction properties [11,13–15]; the presence of V_O's is also one of the main hypotheses to explain the appearance of parent properties such as magnetism. Another important field of research, which is currently driving lots of effort of research, concerns the understanding of the resistive switching mechanisms when an electric field is applied, as they could be used to design future memories known as resistive random access memory (ReRAM). Such resistive switching has already been evidenced experimentally in metal/$SrTiO_3$ heterostructures and for these processes again the presence of the V_O's is the main factor [16–18].

In the formation of a Schottky barrier [19], without considering the interaction (in terms of charge exchange or atomic relaxation) between the metal and the oxide layer, i.e., in the Schottky-Mott limit [20,21], the band alignment is determined by the work function of the metal and the ionization potential of the oxide. The real Schottky barrier height (SBH) may be however mostly dependent of the so-called Fermi level pinning arising from two different mechanisms, an intrinsic contribution coming from the appearance of metal-induced gap states (MIGS) associated with the chemical bonding between the metal and the oxide and an extrinsic contribution which can originate from defects such as oxygen vacancies [19,22].

*remi.arras@cemes.fr

Several studies have already been published on the growth of metallic layers on STO and the formation of Schottky barriers. The electronic and structural properties have also been addressed theoretically by the mean of first-principles calculations [22–24]. As for the previously discussed properties, for the SBH formation also the complex role of structural defects and in particular of oxygen vacancies may be expected to be crucial, but has however not been extensively studied numerically.

The numerous theoretical studies of oxygen vacancies in STO and near its surfaces show the complexity of such a system [24–38]. Calculations of the V_O stabilities near STO surfaces have allowed us to conclude that they are expected to be located close to the surface and preferably in TiO_2 atomic layers, suggesting a possible migration of vacancies during the growth [24,36,38], which could result in V_O clusterization [39]. Thanks to nudged elastic band calculations, Brown *et al.* [38] found that the V_O diffusion is kinetically controlled and they calculated a diffusion barrier energy of 0.7 eV to move the V_O from the SrO subsurface layer to the TiO_2 surface layer. For the surfaces again, Ma *et al.* [24] found that V_O can induce oxygen octahedra rotations (OORs) only when localized in a TiO_2 atomic layer, which can help stabilize the defect in such an atomic plane. They also extended their study to the Au/STO(001) interfaces, for which their results are qualitatively found to be the same. The *n*-type SBH at the Au/STO interface, defined as the difference between the conduction band minimum (CBM) energy and the Fermi level energy E_F, is calculated to be 1.0 (0.6) eV for a SrO (TiO_2) termination. These values are strongly reduced to 0.2 (0.1) eV when a V_O is introduced in the interface atomic layer and the STO layer can become conducting, forming an ohmic-type contact, when the vacancy is located further from the interface.

Catrou *et al.* [8] experimentally studied Fe/STO(001) interfaces. Their samples displayed mostly interfaces with a TiO_2 termination, the SrO termination covering approximately 10% to 20% of the surface area. The interface formation with the metallic electrode is made during the deposition of the first 10 monolayers (ML) of Fe. Below this value, the CBM appears to be below the Fermi level, which corresponds to a metallization of STO, while above a thickness of 15 ML, a SBH of 0.05 ± 0.07 eV is stabilized. From current-voltage measurements, a SBH lower than 0.25 eV is estimated. These experimental results do not seem directly comparable with theoretical calculations performed on Cr/STO interfaces, which rather suggested SBH of 1.3 (1.0) eV for a TiO_2 (SrO)-terminated interface. [22] The hypothesis that the SBH could be reduced due to the presence of oxygen vacancies in STO has been advanced by Catrou *et al.* to explain such a discrepancy, which we have tried to verify with the present study.

In the following we provide a theoretical insight of the SBH formation at the Fe/STO(001) interface. We will first give an as global as possible overview of the electronic structure, intimately linked with the variation of the magnetic properties at this interface, as a function of the atomic structure: Three different structural parameters will be envisioned, i.e., (1) the interface termination, (2) the presence of oxygen vacancies, and (3) the potential oxidation of the Fe layer near the interface. Considering this set of parameters, we aim at understanding the lowering of the SBH measured experimentally at the Fe/STO(001) interface. All these results have been obtained by taking explicitly into account the interfaces; a comparison with bulk calculations and a discussion of the calculation parameters is given in the Appendixes, as well as a full description of the magnetic properties calculated in the presence of an oxygen vacancy.

II. DETAILS OF THE CALCULATIONS

We performed first-principles calculations based on the density functional theory (DFT) using the Vienna *ab initio* simulation package (VASP) [40,41] with the projector augmented-wave method [42] and a cut-off energy of 500 eV. The generalized-gradient approximation proposed by Perdew, Burke, and Ernzerhof and revised for solid (PBESol) was used for the exchange-correlation functional [43]. A "$+U$" correction [44] was applied to the d electrons of Ti atoms, with a U_{eff} ($= U - J$) value of 8.0 eV to improve the band-gap calculation and as proposed in Refs. [16,23]: Using such a parameter, we calculated a band gap around the Fermi level E_F of 2.83 eV that is 1 eV higher than with the PBESol approximation alone and closer from the experimental value of 3.2 eV. A comparison of the electronic properties of the bulk STO in the presence of oxygen vacancies is given in Appendix A with a discussion of the influence of some calculation parameters, including the choice of U_{eff}.

The lattice parameter of bulk STO has been calculated to 3.950 Å with the PBESol + U method, i.e., 1.15% higher than the experimental value. The atom coordinates and lattice parameters have been optimized until all forces are below 5 meV/Å. For the interface calculations, a symmetric slab was used with a (2×2) lateral dimension; in Appendix A we also discuss the dimensionality effects linked to the limited size of our supercells. The lattice parameter was fixed to the bulk equilibrium value corresponding to the chosen approximation for the exchange-correlation functional. The slab thickness in the [001] direction was of 10.5 unit cells of STO (that is 21 atomic ML), with two TiO_2 or SrO-terminated interfaces, each one associated with a 5-ML-thick Fe layer. Fe atoms located at the interface are placed on top of the oxygen atoms for the TiO_2 termination, which has been found to be the most stable configuration for many metal/perovskite systems [45–47]; they are located on top of oxygen and Sr atoms for the SrO interface. Each Fe surface is separated by at least 15 Å of vacuum.

Finally, the first Brillouin zone was sampled with a $8 \times 8 \times 1$ Monkhorst-Pack grid [48] for the structural optimization and the electronic structure is then calculated with a slightly denser mesh of $10 \times 10 \times 1$. The SBH are calculated using the layer-resolved densities of states (LDOS) [24,49,50]. More details about the calculation of the SBH are given in Appendix B.

III. GENERAL PROPERTIES OF THE Fe/$SrTiO_3$(001) INTERFACES

A. Dependence on the interface termination

We first analyze the properties of perfect Fe/STO interfaces with a TiO_2 or SrO termination.

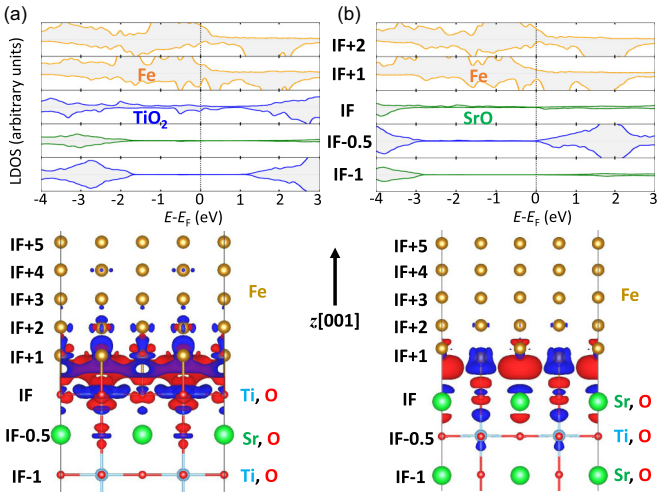

FIG. 1. (Top) Layer-resolved densities of states (LDOS) of the (001) atomic planes and (bottom) charge density difference near the (a) TiO_2- and (b) SrO-terminated interfaces (IF). The charge density difference is defined by the formula $\Delta\rho = \rho_{HS} - (\rho_{STO} + \rho_{Fe})$, where ρ_{HS}, ρ_{STO}, and ρ_{Fe} are, respectively, the charge densities for the heterostructure, the STO, and the Fe layers. Red area corresponds to a positive $\Delta\rho$, while blue area is for negative values.

We define the cleavage or separation energy E_{sep} as the energy difference per surface area A between the ground state total energy of the heterostructure E_{HS} and the sum of the ground state energies of the two relaxed Fe and STO layers taken separately and respectively denoted as E^{Fe}_{layer} and E^{STO}_{layer}:

$$E_{sep} = \frac{1}{2A}\left[E_{HS} - \left(E^{Fe}_{layer} + E^{STO}_{layer}\right)\right]. \quad (1)$$

We calculated that this separation energy is $E_{sep} = -7.34\,\text{eV nm}^{-2}$ and $E_{sep} = -5.84\,\text{eV nm}^{-2}$, respectively, for a TiO_2 and a SrO termination, suggesting that the former is indeed more stable.

The presence of the interface induces low structural distortions. The calculated Fe-O distances are 1.914 (1.983) Å at the TiO_2 (SrO)-terminated interface and the Ti-O bond lengths near the interfaces are only increased by 0.5% in comparison to the bulk value. Our calculated Fe-O distance at the interface is in agreement with a previously reported value of 1.961 Å [51]. The oxygen-cation buckling, defined as $\Delta z = z(\text{cation}) - z(\text{O})$ with z the coordinate along the [001] direction, is a quantity which can be related to the emergence of a local electric polarization. A slight buckling of $\Delta z = 4 \times 10^{-2}$ Å is observed in the interface layer with the TiO_2 termination, and of $\Delta z = 2.5 \times 10^{-1}$ Å for the SrO interface. Still for the SrO-terminated interface, this same buckling is of 3×10^{-2} Å in the subinterface TiO_2 layer, while it rapidly tends to 0 Å for the TiO_2-terminated interface. Finally, when looking in more detail the atomic structure near the interface [see the bottom of Fig. 1(b)], it is also interesting to notice that the SrO termination induces more distortions in the first Fe atomic layer near the interface (denoted IF + 1), which can be easily explained by considering the two different atomic sites of this layer, half of the atoms being bonded to oxygen atoms and consequently attracted toward the STO layer, the other half of the interface Fe atoms being on top of a Sr atom, and then repelled from the interface.

The calculated electronic structure at the Fe/STO interface is in agreement with a previous report from the literature [51] and shares different similarities with parent interfaces between a Fe or Co electrode and a ferroelectric perovskite with a TiO_2 surface termination [52–54]. The bottom of the conduction band in STO has mostly a Ti-d character. Because the d bands of Fe atoms are more than half occupied, most of the transferred electrons have a minority spin momentum. The LDOSs of Fig. 1(a) show indeed the appearance of minority-spin Ti-$d_{xz,yz}$ states in the band gap, just around the Fermi level and well localized at the interface, which has for consequence to induce a negative spin magnetic moment of $-0.32\ \mu_B$ on the Ti atom. This induced spin magnetic moment on the Ti atoms goes in hand with an increase of the spin magnetic moment of the interfacial Fe atoms, from an averaged value of $2.12\ \mu_B$ in the center of the layer up to $2.31\ \mu_B$ at the interface. For the SrO interface, on the contrary, we do not observe any clear MIGS in the STO band gap near the interface [Fig. 1(b)]. We calculated low induced magnetic moments on the oxygen and Ti first neighbors of the interface, of approximated values of $0.05\ \mu_B$, and almost no variation of the spin magnetic moment for the Fe atoms on top of the hollow atomic site; on the contrary, the Fe atoms bonded to the oxygen atoms at the interface undergo a high increase of their magnetic moment to $2.91\ \mu_B$, which is $0.13\ \mu_B$ higher than the magnetic moment of the Fe atoms at the bare surface and $0.79\ \mu_B$ higher than the bulk value. Finally, as it will be discussed later, we calculated the formation of an internal electric field of approximately $-0.01\,\text{V Å}^{-1}$ for the TiO_2-terminated interface, which can result from the charge transfer at the interface, while it is almost null for the SrO termination.

Another way to tackle the charge transfer through the interface is by performing the Bader charge analysis [55–57]. The formal electric charge carried by the Ti cation in STO is $+4e$, by approximating this compound to a ionic crystal. We calculated a Bader charge of $+2.33e$ for the Ti atoms in the bulk compound. The calculated value in the center of our supercell is similar ($+2.25e$), but it decreases to $+2.10e$ near the TiO_2 interface, indicating an increase of the number of electrons, while no change is noticed for the SrO interface. The charge transfer, due to the proximity between the Ti and Fe atoms at the TiO_2 interface, can be noticed in the charge density difference (CDD) plotted in Fig 1(a), i.e., the charge difference between the complete heterostructure, and the sum of the charge densities of the two Fe and STO layers with the same atomic structure. We can see in this figure that we have large positive red areas above the interfacial Ti atoms, with a clear out-of-plane component, which is consistent with the populating of the $d_{xz,yz}$ bands. The establishment of the chemical bonds between Fe and oxygen atoms may be also noticed due to the charge transfer from the negative blue areas with a d_{z^2}-orbital shape and located on the Fe atoms to the red areas with p_z-orbital shapes located on the oxygen atoms in the interfacial TiO_2 atomic layer. In the case of the SrO termination [Fig. 1(b)], most of the charge transfer occurs from the Fe atoms linked to one oxygen anion to this same oxygen anion, which is highlighted by the spin polarization of out-of-plane orbitals. We can in particular notice alternating

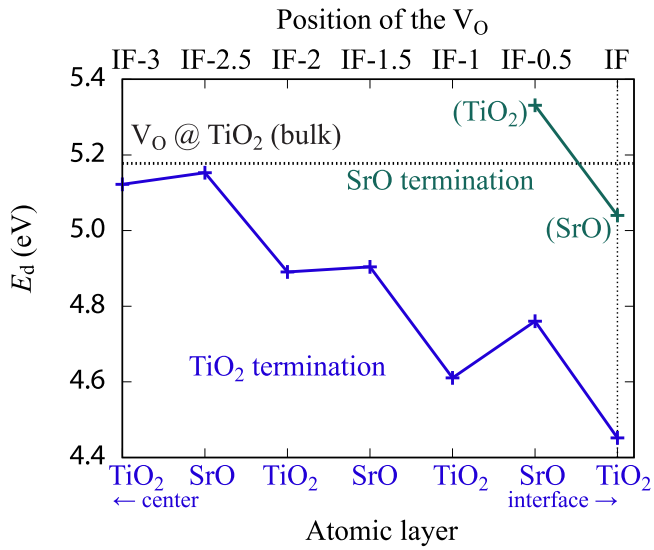

FIG. 2. The formation energy of the oxygen vacancy as a function of its position according to the interface for the TiO_2-terminated (blue) and SrO-terminated interface (green). The black dotted line corresponds to the formation energy (5.18 eV) of a V_O calculated in a $2 \times 2 \times 5$ bulk supercell and the V_O located in a TiO_2 (001) atomic layer. When the V_O is located in a SrO layer, the formation energy increases up to 5.68 eV.

negative and positive CDD in the (001) plane of the interface, which can directly be related to the structural distortion: Negative CDD is associated with Fe atoms bonded to oxygen atoms with which they experience a charge transfer, while the positive CDD can be seen in the interstitial zone below the Fe atoms which are repelled from the interface.

B. Effect of the oxygen vacancies

We will now discuss the effect of the presence of one V_O as a function of its location with respect to the interface. We will mostly focus our discussion on the case of the most stable TiO_2-terminated interface.

a. Formation energy: Figure 2 displays the formation energy [58,59] E_d of one oxygen vacancy as a function of its position in the successive (001) atomic layers and calculated following the formula

$$E_d = \tfrac{1}{2}[E_{HS+nV_O} - E_{HS} - n(\mu_{O_2} + \Delta\mu_{O_2})], \qquad (2)$$

with E_{HS+nV_O} and E_{HS}, respectively, the ground state energy of the heterostructures with and without oxygen vacancies V_O and which are formed by two equivalent interfaces. μ_{O_2} is the chemical potential of an O_2 molecule and n corresponds to the number of oxygen vacancies. Because we will only be interested in studying the variation of formation energy as a function of the position of the vacancies and for the sake of simplicity, we neglected the term $\Delta\mu_{O_2}$, which depends on the growth conditions and we only considered the formation of electrically neutral oxygen vacancies. Some results considering charged V_O are described in Appendix A.

As calculated by Ma *et al.* for a Au/STO(001) interface [24], we found that the position of the oxygen vacancy is more stable when the vacancy is located near the interface

TABLE I. . Formation energies E_d calculated using Eq. (2). The energies are given as a function of the position of two oxygen vacancies, which are located, respectively, in atomic layer 1 and layer 2. The label IF corresponds to the TiO_2-terminated interface, as defined in Fig. 1(a). The distances between the two oxygen vacancies V_O are given as a function of an approximated cubic lattice parameter a (which is fixed to the bulk value for in-plane directions and may vary for out-of-plane directions). The case of two V_O located at the interface and at a distance of $\simeq 2a$ is strictly equivalent to the previously discussed case with one V_O in the 2×2 lateral supercell.

Layer 1	Layer 2	$d(V_O - V_O)$	E_d (eV/V_O)
IF	IF	$\simeq a/\sqrt{2}$	4.17
IF	IF	$\simeq a$	4.24
IF	IF	$\simeq 2a$	4.45
IF	IF-0.5	$a/\sqrt{2}$	4.46
IF	IF-0.5	$\simeq \sqrt{3}a/2$	4.57
IF	IF-1	$\simeq a$	4.54

and in a TiO_2 layer: The formation energy increases by 0.2–0.3 eV from the first to the second atomic ML away from the interface, and by approximately 0.8 eV further. Oxygen vacancies having a lower formation energy near interfaces have already been predicted in several metal/oxide systems and may be partly attributed to the presence of the partially occupied MIGSs which allow us to accommodate the excess of electrons released by the V_O (see Ref. [60] and references therein). As discussed later, the atomic structure near the interface can undergo different kinds of structural distortions (OOR or buckling), depending on the position of the V_O; in addition to the symmetric slab with limited thickness which was used, this makes difficult any comparison between the calculated formation energies of the V_O in the slab and in the bulk compound.

We extended the previous calculations to the formation energy E_d of two V_O's as a function of the distance separating them. Because we found that the interfacial TiO_2 layer (IF) is the most suitable position for the formation of a V_O, we considered that one of the two vacancies is necessarily in this layer. We can easily see from Table I that the two V_O's present a clear tendency to clusterize, with the lowest formation energy $E_d = 4.17$ eV calculated when the two V_O's are both in the IF layer and at the minimum distance of $a/\sqrt{2}$, i.e., 0.28 eV/V_O lower than the formation energy calculated with only one V_O. Using a $3 \times 3 \times 4$ supercell, Jeschke *et al.* also found that a tendency of the V_O's to clusterize in the perpendicular direction near a TiO_2-terminated surface, while they found on the contrary that the V_O's tend to be homogeneously separated when located inside the same parallel surface layer [39].

b. Atomic structure relaxation: After optimization of the atomic structure, we found that the averaged interplane distance in STO is reduced by 3.8% in the vicinity of the perfect interface compared to the bulk equilibrium value. This interplane distance increases to recover the bulk value from 3 ML away of the interface. Including an oxygen vacancy will add some distortions, inducing oscillations of these interplane distances. As shown in Fig. 3(a), this change of out-of-plane

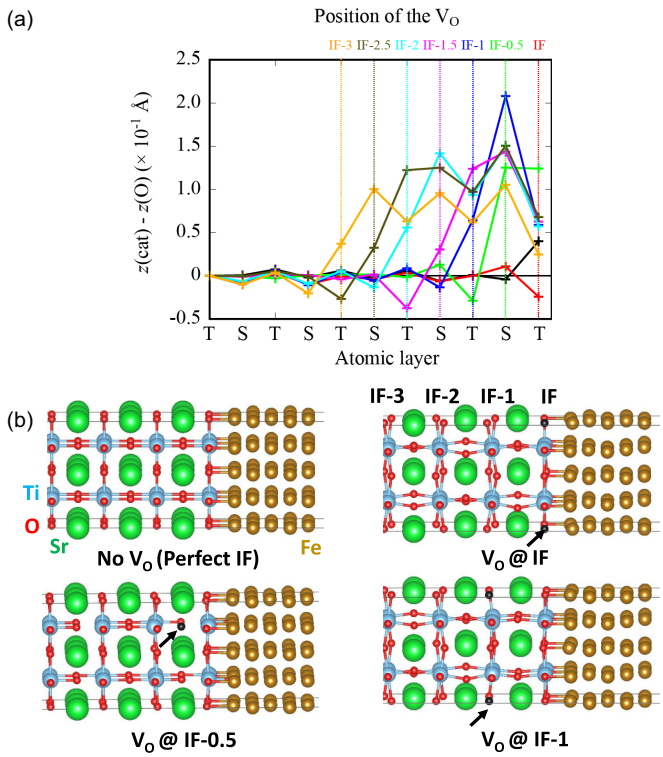

FIG. 3. (a) Cation-oxygen buckling; the black curve corresponds to the reference structure without V_O. The letters "T" and "S" represent, respectively, the TiO_2 and SrO atomic layers. (b) Atomic structure of the $Fe/SrTiO_3$ without any oxygen vacancy V_O and with one oxygen vacancy in three different positions.

lattice parameter is accompanied by a cation-oxygen buckling between the interface and the atomic plane which contains the oxygen vacancy: This buckling Δz is characterized by a positive variation of the z[001] coordinate of approximately 0.13 Å, which is approximately of the same magnitude that can be calculated for the ferroelectric bulk oxide $BaTiO_3$.

In addition to the cation-oxygen buckling, when the oxygen vacancy is located in a TiO_2 plane, we can notice the appearance of OORs in the planes located after the TiO_2 vacancy plane, toward the center of the slab [see Fig 3(b)]. As it is discussed in Appendix A, the presence of OOR is also noticed in the bulk compound [35] due to the symmetry reduction induced by the V_O and we can expect that such distortions help to reduce the formation energy of the defects, explaining why TiO_2 atomic layers are an energetically more favorable location for a V_O than SrO layers, as proposed by Ma *et al.* in the case of $SrTiO_3$ surfaces [24]. When analyzing Fig. 2 we can see in particular that the energy-formation difference between a TiO_2 or a SrO location decreases as we are moving far away from the interface. Such an observation may be directly linked to the proximity to the interface, but can also be a result of the finite size of our slab and the special symmetrical geometry we chose to use: When we move the two symmetric images of oxygen vacancies toward the center of the slab, we reduce the number of atomic planes which can host the OOR. This potential calculation artifact, with the appearance of cation-oxygen buckling, explains why moving the V_O toward the center of the slab does not allow us to recover the two formation energies (depending on which layer is hosting the V_O), different by 0.5 eV for a $2 \times 2 \times 5$ bulk supercell (see Appendix A and Fig. 2).

c. Electronic structure: Associated with the atomic distortions and the cation-oxygen buckling Δz, we have the creation of electric dipoles and it is possible to calculate a local electric polarization P_i by using Born effective charges Z^*:

$$P_i^l = \frac{e}{\Omega} \sum_{\kappa} Z^*_{z,i,\kappa} (\delta z)_{i,\kappa}, \tag{3a}$$

$$P_i = P_i^l + \frac{1}{2}\left(P^l_{i-0.5} + P^l_{i+0.5}\right), \tag{3b}$$

with P_i^l the contribution to the electric polarization along z[001] of the atomic layer i and calculated by summing the Born effective charges $Z^*_{z,i,\kappa}$ of the κ atoms forming the layer, multiplied by the variation of the coordinate z according to the middle between the averaged position of the adjacent layers: $(\delta z)_{i,\kappa} = \langle z \rangle_{i,\kappa} - \frac{\langle z \rangle_{i-0.5} + \langle z \rangle_{i+0.5}}{2}$. The volume of the unit cell Ω is also expressed as the volume delimited by these two adjacent layers, which yields to $\Omega = a^2 |\langle z \rangle_{i+0.5} - \langle z \rangle_{i-0.5}|$. In Fig. 4(a) we consider an in-plane-averaged electric polarization P_i, which follows the expression of Eq. (3 b) and which shares some similarities with the equation proposed in Ref. [50]. The Born effective charges calculated for the bulk STO compound are $Z^*_{z,\mathrm{Ti}} = 5.93e$, $Z^*_{z,\mathrm{Sr}} = 2.55e$, $Z^*_{z,\mathrm{O}^{\parallel}} = -1.88e$, and $Z^*_{z,\mathrm{O}^{\perp}} = -4.75e$, respectively, for the Ti, Sr, in-plane oxygen, and out-of-plane oxygen atoms. We can see that we obtain an almost constant electric polarization from the atomic layer where the V_O is located and pointing toward the interface. The value of this polarization P_i decreases almost regularly between 35 and 19 $\mu C\,cm^{-2}$, when moving the V_O from the TiO_2(IF-1) to the TiO_2(IF-3) atomic layer. The V_O in the interface plane (IF) appears to be a particular case for which the charge transfers induce locally a reversal of the polarization sign.

Figure 4(b) is complementary to the calculated local electric polarization. It presents the $1s$ core energy levels of the oxygen atoms compared to their calculated bulk value: $\Delta E_{1s} = E^i_{1s} - E^{\mathrm{bulk}}_{1s}$. The relative energy of the core levels is shifted between each atomic layer i when going away from the perfect TiO_2-terminated interface (black curve), which corresponds to a band bending and is a consequence of the appearance of an internal electric field, oriented toward the center of the slab and evaluated to $E_{\mathrm{field}} = \frac{\delta(\Delta E_{1s})}{e\delta z} \sim -0.01\,\mathrm{V\,Å^{-1}}$. The presence of the V_O at the interface reduces the value of this electric field, while a net positive electric field is created when the V_O is located in the next layers, with a value of approximately $+0.045$ V Å^{-1}, when in the TiO_2(IF-3) layer. This estimated value of the electric field would correspond to an averaged value of electric polarization of $P = \varepsilon_r \varepsilon_0 E_{\mathrm{field}} \sim 16\ \mu C\,cm^{-2}$ (considering a calculated relative permittivity of $\varepsilon_r = 39.4$), i.e., a value close to the previous estimation of P_i. It is also interesting to note that the formation of this internal electric field may partly explain why the neutral oxygen vacancies have a higher formation energy far from the interface, because this field will add an electrostatic contribution to the total energy equal to ezE_{field}, as discussed in Ref. [61]. If this assumption is correct, we can emit the hypothesis that the formation of positively

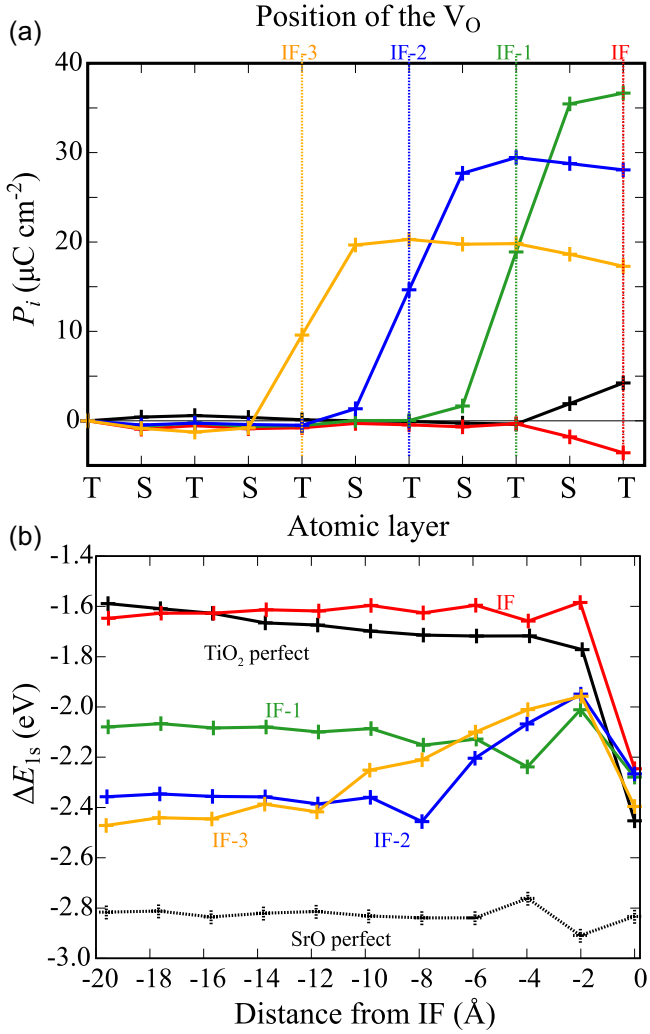

FIG. 4. (a) Local electric polarization P_i as a function of the position of the V_O and of the atomic layer i (T is for TiO_2 and S for SrO) and (b) variation of the O-1s energy level as a function of the distance to the interface. The value ΔE_{1s} is given according to the energy level calculated for the bulk STO.

charged V_O, which we only calculated for the bulk oxide (see Appendix A), could maybe be more favorable away from the interface, in order to reduce the amount of localized charges.

The variations of the spin magnetic properties described in Appendix C are witnesses of the structural and electronic modifications arising from the presence of the V_O, and thanks to their study, it is possible to obtain a guess of the charges localized near the V_O or transferred to the interface. From our calculations we have found that when the V_O is in the TiO_2 interface layer, the partially occupied MIGSs trap the 2 electrons released by the neutral vacancy (i.e., 0.5 electron/Ti atom). When the V_O is located in atomic layers further from the interface, only a part of the released charges stays localized in the TiO_2 layer first neighbor of the vacancy, the other part being transferred to the TiO_2 interface layer as a result of the electric polarization. The further the V_O is from the interface, the lower the amount of transferred charges; which is consistent with the decrease of the averaged absolute value of the spin magnetic moment of the interfacial Ti atoms.

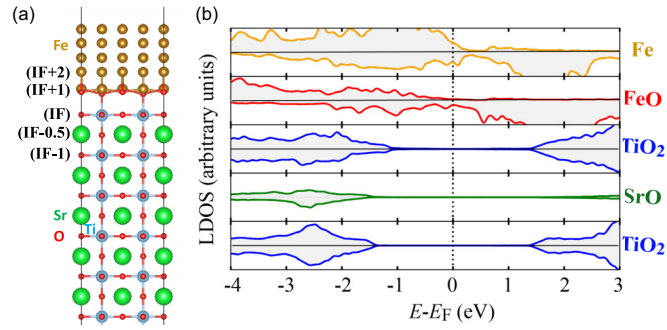

FIG. 5. (a) Atomic structure of the oxidized TiO_2-terminated $Fe/SrTiO_3$ interface and (b) the corresponding LDOS of the interfacial layers. The calculations have been performed with a U_{eff}-dependent correction applied to the 3d bands of Fe atoms.

Taking again the example of the oxygen vacancies located in the TiO_2(IF-3) atomic layer, we can from the calculated spin magnetic moment consider that this TiO_2(IF-3) layer is charged with $Q_{V_O} = -1.06e$, while the TiO_2(IF) layer possess an excess of $Q_{IF} = -2.15e$. With the model of a plane capacitor and doing the approximation that the charges are uniformly spread in the atomic layers, we obtain Eq. (4)

$$E_{field} = \frac{Q_{V_O} - Q_{IF}}{2\varepsilon_r \varepsilon_0 A} \tag{4}$$

and we can calculate that these charges would lead to the creation of an internal electric field of $E_{field} = +0.040$ V Å^{-1}, which is consistent with the previous estimation obtained by fitting the variation of the core state energy.

C. Effect of the Fe-layer oxidation

During the growth of the Fe layer, the formation of oxygen vacancies in STO can be the result of the migration of oxygen atoms toward the interface, partially oxidizing the metal layer [12,62], in our case the Fe layer. The formation of an FeO(IF + 1) oxide at the TiO_2-terminated interface can also be controlled by growing the layer in an oxygen-rich atmosphere. We considered here the simple structure for which the atomic Fe layer at the interface is fully oxidized, forming a two-dimensional FeO layer in between Fe and STO; the added oxygen atoms are located such that they form a two-dimensional face-centered square lattice with the Fe atoms [see Fig. 5(a)].

Our calculations show that the magnetic coupling in the FeO layer is ferromagnetic, with an energy difference of −0.17 eV/formula unit (f.u.) of FeO [−0.22 eV/f.u. if we add a U-dependent correction with U_{eff}(Fe,3d) = 4 eV]. The oxidation is accompanied by a large increase of the Fe spin magnetic moment to 3.08 μ_B and the induction of a magnetic moment of 0.18 μ_B on the oxygen atoms of the same layer. On the contrary, the Ti and O atoms of the interfacial TiO_2 layer only display spin magnetic moments lower than 0.05 μ_B, which suggests a lower interaction between these atoms and the Fe layer. This statement is consistent with the larger Fe-O interatomic distance (2.459 Å) calculated for this oxidized interface, and which results in the quasidisappearance of the gap states in the LDOS [as shown in Fig. 5(b)], in

accordance with the calculated electronic structure reported at the oxidized Co/Pb(Zr,Ti)O_3 interface [54].

IV. SCHOTTKY BARRIER FORMATION

Having discussed the main properties of the Fe/STO interfaces, we can now address the problem of the SBH formation.

We calculated a work function of 4.01 eV for the Fe layer (the experimental value is approximately 4.67–4.81 eV [63]). By using the calculation methods described in Ref. [22], we also obtained an ionization potentials of 5.30 and 3.78 eV for the relaxed STO surfaces, with respectively a TiO_2 or SrO termination. According to the Schottky-Mott rule, i.e., without considering the band alignment and the interface atomic structure relaxations, we would expect the Fermi level of the Fe to be located close to the middle of the band gap of STO for a perfect TiO_2-terminated interface, giving a *p*-type SBH of 1.29 eV, while it should be below the valence band maximum for the other termination, then creating an Ohmic contact. However, calculating directly the SBH by using the LDOS provides a somewhat different scenario for the second interface: We calculated a *p*-type SBH of 1.61 eV and a *n*-type value of 1.23 eV (1.59 eV if we consider the experimental band gap of 3.2 eV) for the TiO_2-terminated interface; for the SrO interface, the calculated *p*-type SBH is almost equal to the calculated band-gap energy, i.e., 2.80 eV, and we then found an almost null, but not vanishing, *n*-type SBH of 10 meV (≈ 0.4 eV with the experimental band gap). The reported presence of 10%–20% of SrO termination could thus possibly corroborate the large reduction of the *n*-type SBH measured experimentally (0.05 ± 0.07 eV) [8]. For this last interface, the bonding between the two layers at the interface and the relaxation of the atomic structure are critical to obtain the Schottky behavior. Calculating the ionization potential for a STO layer with the atomic structure of the interface, we indeed obtain an increase of 0.5 eV of its value, compared with the relaxed SrO surface.

From a more technical point of view and still for the SrO-terminated interface, we should mention that, on the contrary to the TiO_2-terminated interface, the calculation of the *p*-SBH is also strongly dependent on the U_{eff} parameter used for the calculation: Increasing the U_{eff} value from 0 to 8 eV lowers the occupied valence states regarding the Fermi energy and thus increases the *p*-SBH by approximately 0.8 eV. Qualitatively, the SrO-terminated interface displays lower *n*-SBH (by 0.5 to 1.5 eV) than the TiO_2-terminated one, which is consistent with the calculations displayed in Ref. [22] for the Cr/STO interface. For the interface between the noble metal Au and STO, an opposite behavior has been calculated with a *n*-type SBH higher for the SrO interface (1.0 eV) than for the TiO_2 termination (0.6 eV) [24].

When a V_O is introduced in the structure and is located in the TiO_2 interface layer, the SBH is unaffected if compared to the nondefective interface because the modifications of the electronic structure remain mostly localized at the interface. When the vacancy is moved toward the center of the slab, we have a decrease of the *n*-type SBH: This decrease is drastic, by 0.7 eV, from the interface (IF) to the first-neighbor monolayer (IF-0.5), before following a quasilinear variation between the atomic layers IF-1 and IF-3, where it reaches a value of 0.38 eV.

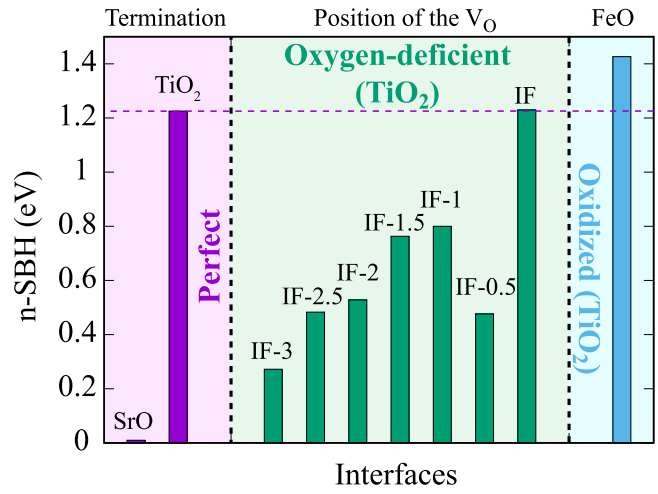

FIG. 6. Summary of the different *n*-type Schottky barrier heights (SBHs) calculated for the perfect SrO- and TiO_2-terminated interfaces (left) and for the TiO_2-terminated interface with an oxygen vacancy (center) or an oxidized FeO layer (right).

If we consider now the SrO interface termination for which the SBH is already strongly reduced without any defects, the presence of a V_O in the SrO interfacial layer slightly increases the calculated *n*-SBH from 10 to 75 meV, while the V_O in the TiO_2 subinterface layer induces some band crossing of the Fermi level for TiO_2 atomic layers in the center of the slab, which indicates that the V_O combined with such interface termination are more likely to induce an ohmic behavior.

As shown in the right part of Fig. 6, we calculated a higher *n*-type SBH, of 1.39 eV, when the first Fe layer is fully oxidized and the interface termination is FeO/TiO_2. This value was obtained by applying a U_{eff} correction of 4 eV on the *d* orbitals of the Fe atoms from the FeO layer; without this correction, a very close value of 1.47 eV was found, which indicates that this correction does not change significantly the result. Such a result is important as it would suggest that both healing the oxygen vacancies and oxidizing the interface could contribute to an increase of the *n*-type SBH.

V. CONCLUSION

We performed first-principles calculations based on the DFT + U to investigate different configurations of Fe/STO interfaces and to try to define which are the key parameters which would explain the measured low *n*-type SBH. Our results have been discussed regarding the choice of the different computational parameters and their limitation.

We first found that the termination of a perfect interface (either Fe/TiO_2 or Fe/SrO) appears to be the most detrimental factor to get high *n*-type SBH and the most plausible scenario to explain the experimental measurements of Ref. [8], the SrO termination leading to an almost zero barrier. According to our calculations, such termination, if combined with some additional defect like oxygen vacancies, would inevitably induce an ohmic behavior.

Providing that a TiO_2 termination is stabilized, oxygen vacancies may also induce some modifications of the SBH, but these modifications are expected to be more limited. We indeed found that, as in the case of the Au/STO interface [24], the creation of a neutral V_O is energetically more favorable in the TiO_2 interface layer, where the partially occupied gap states, resulting from the chemical bonding with the Fe layer, can help us to accommodate the charges released by the defect. If the formation or migration of V_O is still possible in atomic layers away from this interface layer, these locations are energetically less favorable; in that case, a part of the charges given by the V_O can stay localized on Ti atoms near the defect position and in addition distort the lattice and reduce the *n*-type SBH.

Healing the oxygen vacancies by heating post treatment or by growing the samples under an oxygen-rich environment would then help us to preserve higher *n*-type SBH. In addition, we have found that oxidizing the first Fe layer near the interface would improve this value.

The control of the $Fe/SrTiO_3(001)$ interface would thus provide an interesting opportunity to design magnetic Schottky junctions with tunable barrier heights and which could be coupled with innovative systems, like multiferroics with a magnetoelectric coupling controllable via the V_O's or surfaces/interfaces hosting a (spin-polarized) two-dimensional electron gas.

ACKNOWLEDGMENTS

This work was granted access to the HPC resources of CALMIP supercomputing center under the allocation 2019 and 2020-p19004.

APPENDIX A: BULK CALCULATIONS

For comparison purposes with the interface properties, we propose in this Appendix to describe the calculated bulk physical properties. This discussion is also the opportunity to address the question of the effect of the choice of U_{eff}. Bulk properties such as atomic distortions, formation energies, or electronic properties can vary significantly as a function of the considered initial structure and the choice of the exchange-correlation approximation. It was for example shown that there is normally a necessity to use large supercells (larger than $3 \times 3 \times 3$) to avoid too strong interaction between the periodic images of the vacancy, and that the formation energy can vary by more than 1 eV between a cell of 40 atoms and one of 320 atoms [26,28], while some studies reported a low variation of only 0.1 eV between a $2 \times 2 \times 2$ and $3 \times 3 \times 3$ supercell. If early studies have confirmed the presence of gap states using DFT + U or hybrid functionals [25,29,30,32,34], Choi *et al.* have suggested that such states disappear when using sufficiently large supercells (625–1080 atoms) with a cubic structure [35]. The same authors also proposed that a local antiferrodistortive-like structure could be induced by oxygen vacancies, with some associated gap states.

a. Effect of the supercell geometry and size: Our first bulk calculations were performed with the PBESol + U approximation and using $2 \times 2 \times 2$ and $3 \times 3 \times 3$ supercells. With $U_{\text{eff}} = 8$ eV we, respectively, found a formation energy of 5.95 and 5.50 eV. For a comparison with the experience, Catrou *et al.* [8] estimated from photoemission analysis a surface density of vacancies of $\simeq 2 \times 10^{14}$ cm^{-2}, i.e., 1% of vacancies; removing an oxygen atom from a $2 \times 2 \times 1$ supercell corresponds instead to 8.3% of vacancies, and 3.7% for a $3 \times 3 \times 1$ supercell.

We also performed different calculations using a $2 \times 2 \times 5$ supercell with the in-plane lattice parameters fixed to the equilibrium value calculated without any defect and the out-of-plane parameter optimized to minimize the total energy: Such geometry has the same lateral dimension as the slab which has been used to study the interface with a Fe layer and its asymmetry allows us to differentiate the effect of the localization of the oxygen vacancy in a SrO(001) or $TiO_2(001)$ atomic layer. In this condition, the formation energies become 5.18 and 5.68 eV, depending on if the oxygen vacancy is located in a TiO_2 or SrO (001) atomic layer.

The oxygen vacancy, in addition to its effect on the electronic structure, will distort the atomic structure. With the $3 \times 3 \times 3$ supercell, we observe a structure with tilted oxygen octahedra. These tilts are preserved with the $2 \times 2 \times 5$ supercell, only when the V_O is located in the TiO_2 layer, while they disappear otherwise. It is important to note that the 221-$Pm\bar{3}m$ cubic perovskite describing $SrTiO_3$ changes its space group to respectively a 47-*Pmmm* and 123-$P4/mmm$ space group, when the oxygen vacancy is in the TiO_2 or SrO (001) atomic layer. These different space groups result from the periodic and ordered structures we used for our calculations and by symmetry, the OOR are naturally, or not, allowed; a different result could be obtained for a bulk cell with a random distribution of the V_O (hence preserving the cubic symmetry). The calculated OOR angles α and γ are of approximately 7° around the a[100] axis (along the Ti-V_O-Ti direction) and the c[001] axis, which is in agreement with previous reported calculations [35,64], but is significantly larger than angles calculated with the HSE06 hybrid functional [35] or measured experimentally [65], with values closer to 2°. The tilting angle β is almost 0° along the b[010] direction (perpendicular to the Ti-V_O-Ti direction). When the V_O is located in a TiO_2 layer, the $2 \times 2 \times 5$ tilted structure displays an averaged out-of-plane lattice parameter which is 0.2% lower than the in-plane parameter, while the nontilted structure obtained for a V_O in a SrO plane is on the contrary on average 0.2% higher. Phase transition accompanied by the appearance of ferroelectricity or octahedral tilts have already been reported or predicted in STO as a result of strain, doping dimensionality in thin-layer superlattices or near interfaces [23,64,66–69], and have also been proposed in oxygen-deficient STO [24,35].

A neutral oxygen vacancy is expected to release two electrons which will mainly localize themselves on the two Ti atoms first neighbors of the vacancy. A first calculation considering a simple $3 \times 3 \times 3$ supercell shows the appearance of a gap state with d_{z^2} symmetry and associated with a band energy lying 1.17 eV below the conduction band minimum (CBM). This first result is in agreement with results from the literature [25,34]. Considering the $2 \times 2 \times 5$ cell, the d_{z^2} or $d_{x^2-y^2}$ defect states are located approximately 1.65 eV under the CBM, and their energy dispersion in the first Brillouin zone will depend on their symmetry, and thus on the atomic plane in which the V_O is located, as explained later. The

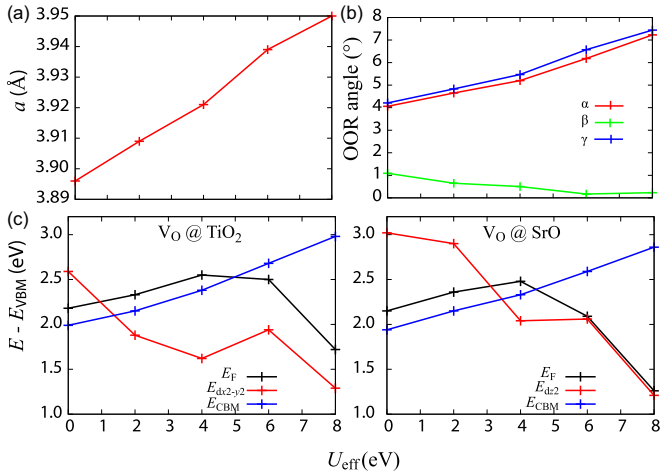

FIG. 7. Calculated $SrTiO_3$ atomic structure parameters and electronic band levels as a function of the U_{eff} parameter: (a) Lattice parameter a calculated for the cubic bulk STO and used as the in-plane lattice parameter for the strained $2 \times 2 \times 5$ bulk supercells and for the interface studies. (b) OOR angles calculated when the V_O is located in a TiO_2 atomic layer in the $2 \times 2 \times 5$ supercell. The angles α, β, and γ are given, respectively, according to the three crystallographic axes a[100], b[010], and c[001], which are parallel to the Ti-O chemical bounds. The values are averaged on every oxygen octahedra not included in the TiO_2 layer containing the V_O. (c) Energy band levels at the Γ high-symmetry point. We define as E_{VBM} and E_{CBM} the energies of the states delimiting the band gap for the nondefective $SrTiO_3$ bulk compound, i.e., respectively, the highest occupied O-p band and the lowest unoccupied Ti-d_{xy} band. The given values are calculated when the V_O is located in a TiO_2 (left) or SrO (right) (001) atomic layer and the red curve corresponds to the energy of the $d_{x^2-y^2}$ or d_{z^2} gap state.

difference of atomic distortion (with the appearance of OOR) does not affect the band-gap width of STO.

b. Variation of the U_{eff} parameter: Keeping the $2 \times 2 \times 5$ cell, we then made a systematic study of the U_{eff}-parameter dependence of our results by varying its value from 0 to 8 eV by steps of 2 eV and we reported in Figs. 7(a) and 7(b) the calculated main characteristics of the atomic structures, which are the calculated in-plane lattice parameters and the OOR angles. As shown in Fig. 7(b), we can notice a significant increase of these angles, which almost double, from 4.1° to 7.3°, when U_{eff} varies from 0 to 8 eV. This goes in hand with an increase of the in-plane-lattice parameter from $a = 3.897$ to 3.950 Å.

The variation of U_{eff} has also an effect on the electronic structure. A summary of the evolution of the band energy at the Γ point near the Fermi level as a function of the value of U_{eff} is given in Fig. 7(c) and a detail of the calculated band structures for some specific values can be visualized in Fig. 8. Three different regimes can be distinguished.

(1) For low U_{eff} values (0–2 eV), the electrons introduced by the neutral V_O will populate the lower conduction bands, which have a d_{xy}, d_{xz}, or d_{yz} character (the minimum of the conduction band corresponding to a d_{xy} band at the Γ high-symmetry point) and they will be delocalized over the whole lattice. This regime is associated with a nonmagnetic state and could be linked to the emergence of a two-dimensional electron gas near a surface or an interface.

(2) For high U_{eff} values (6–8 eV), only one e_g-like band is fully occupied. When the V_O is in a TiO_2 atomic layer, these Ti atoms are located in the same layer, while they are in adjacent layers when the V_O is in a SrO atomic layer; this has for consequences that the occupied defect band will possess a different symmetry, i.e., respectively, $d_{x^2-y^2}$ or d_{z^2}, and have a wider energy dispersion (∼0.4 eV) along the in-plane Γ-X-M directions for the former case. The charges are fully localized between the Ti atoms first neighbors of the vacancy and the defective structure adopts an antiferromagnetic ordering.

(3) For intermediate U_{eff} values (around 4 eV), both (d_{xy}, d_{xz}, d_{yz}) and $d_{x^2-y^2}$ or d_{z^2} bands are partially occupied and a ferromagnetic ordering state appears as the most stable solution (when the oxygen vacancy is in a TiO_2 layer, the $d_{x^2-y^2}$ band is already partially occupied for $U_{\text{eff}} = 2$ eV).

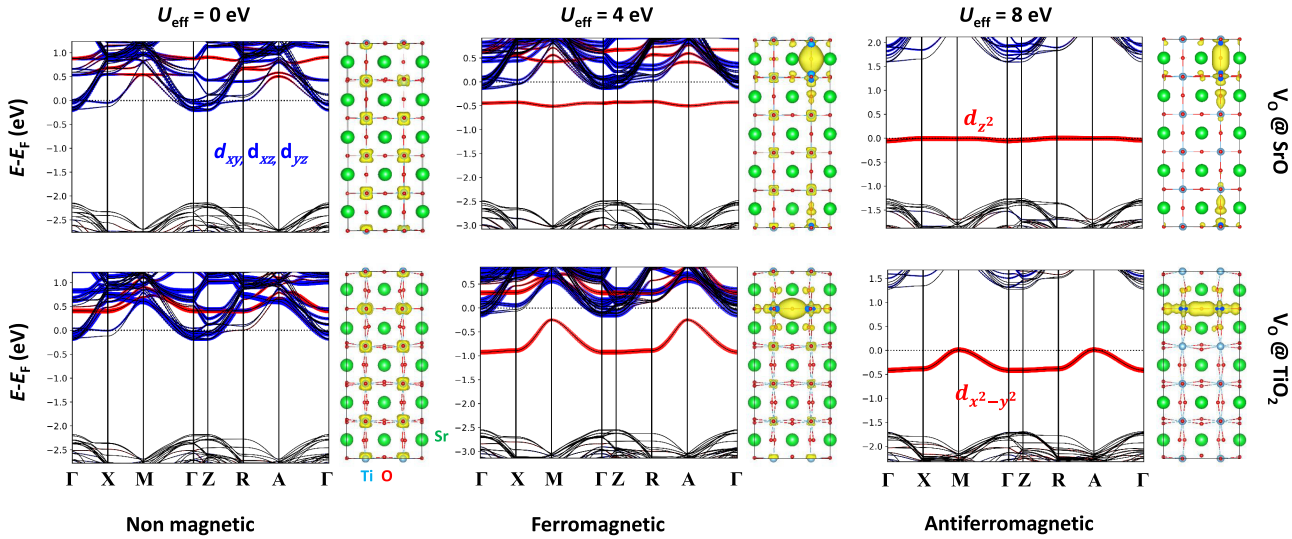

FIG. 8. Band structures and charge densities associated with the electronic states in the energy range between E_F-1.5 eV and E_F, calculated for different values of U_{eff} and the oxygen vacancy located in a TiO_2 or SrO (001) atomic layer.

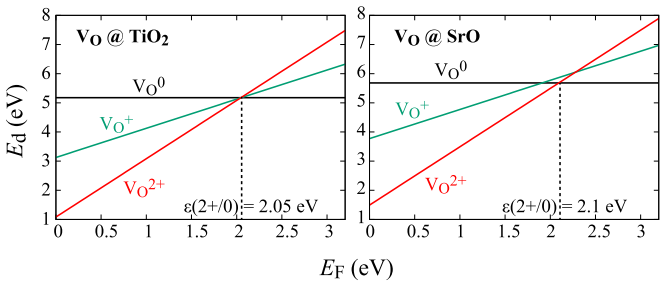

FIG. 9. Formation energies $E_d(V_O^q)$ of an oxygen vacancy located either in a TiO_2 (left) or a SrO (right) atomic layer as a function of the position of the Fermi level E_F. The energies were calculated using the $2 \times 2 \times 5$ bulk supercell.

At this point we can conclude that the defective $SrTiO_3$ compound can be described both as a magnetic or nonmagnetic system, associated with a conductive or insulating regime, depending on the energy-band localization, which can be related to the electronic correlations described by the U_{eff} parameter and by the size of the supercell, that is the oxygen vacancy content. A last critical point which could also promote a regime or another would be the taking into account of a disordered distribution of the V_O, which we did not consider for the sake of simplicity.

In their study, Lin and Demkov Ref. [70] proposed with an Anderson impurity model that one electron of the V_O should occupy a localized hybrid $d_{z^2} + p_z$ in-gap state and the other electron on the first conduction band; however, this magnetic impurity does not produce any net magnetic moment. Such a model would give a result close to our calculation performed for $U_{eff} = 4$ eV, except for the magnetic moment.

Altmeyer *et al.* [71] reported calculations on TiO_2- and SrO-terminated surfaces of $SrTiO_3$ with one or two oxygen vacancies and by using the commonly used values of $U = 5$ eV and $J = 0.64$ eV [72]. They found that the vacancies induce an in-gap state 0.5 to 1.0 eV below the Fermi level, the energy depending on the positions of the vacancies according to the surface, on the surface termination and on the tendency to clusterize. This gap state corresponds to electrons localized on the Ti atoms close to the V_O and are related to Ti spin magnetic moments. Ti atoms located further away are on the contrary associated with delocalized and spin-polarized t_{2g} states, which can experience spin-orbit Rashba effects.

c. Stability of charged defects: For the sake of simplicity, we restrained our interface calculations to the study of neutral oxygen vacancies. This choice seems also reasonable as a first approximation, if we consider that the V_O is most likely to be located in a TiO_2 metallic interface layer. Further from the interface, where the STO remains insulating, the formation of charged oxygen vacancies would be possible. Locally, this would agree with the partial localization of the charges near the defect that we calculated.

The formation energy given in Eq. (2) can be rewritten for one V_O in the bulk and with a charge state q [58,59]:

$$E_d(V_O^q) = E_{bulk}(V_O^q) - E_{bulk} - \tfrac{1}{2}(\mu_{O_2} + \Delta\mu_{O_2}) + qE_F, \tag{A1}$$

with the first terms having a similar meaning than in Eq. (2) and the last term corresponding to the chemical potential of the electric charge. The Fermi level E_F will be now considered as a parameter which can vary from 0 [when it is at the valence band maximum (VBM)] to 3.2 eV, the experimental value of the band gap of STO. The variations of the formation energies $E_d(V_O^q)$ as a function of the position of the V_O and of E_F are given in Fig. 9.

The calculated values shows that when the Fermi level is located close to the VBM, the oxygen vacancies will prefer to be in a charge state $q = +2e$. A transition to a neutral state $q = 0e$ occurs at the energy $\varepsilon(2 + /0) \approx 2$ eV. Independently of the position of E_F, we can see that the formation energy for a V_O is always lower when it is located in a $TiO_2(001)$ atomic layer than in a SrO layer. It is interesting to note that the intermediate state of $q = +1e$ is never stable according to this calculation, unless for E_F near the transition energy $\varepsilon(2 + /0)$. For this state we found that a ferromagnetic coupling with a

TABLE II. *p*- and *n*-type SBH calculated for different values of U_{eff} (all energies are given in eV). The corrected *n*-type SBH is obtained by making the difference between the experimental band-gap energy (of 3.2 eV) and the energy of the calculated *p*-type SBH.

TiO_2 termination									
	SBH →	*p*			Calculated *n*			Corrected *n*	
System	U_{eff} →	0	4	8	0	4	8	0	4	8
Perfect IF		1.45	1.53	1.23	0.31	0.71	1.61	1.75	1.67	1.97
V_O@ IF		1.87	1.87	1.64	0.0	0.42	1.23	1.33	1.33	1.56
V_O@ IF-1.5		1.98	2.41	1.45	0.0	0.0	1.35	1.22	0.79	1.75
V_O@ IF-2.5		2.05	2.50	2.37	0.0	0.0	0.48	1.15	0.70	0.83
V_O@ IF-3		2.08	2.41	2.45	0.0	0.0	0.38	1.12	0.79	0.75
SrO termination									
	SBH →	*p*			Calculated *n*			Corrected *n*	
System	U_{eff} →	0	4	8	0	4	8	0	4	8
Perfect IF		1.97	2.36	2.80	0.00	0.00	0.01	1.23	0.84	0.40

spin magnetic moment of 0.2–0.4 μ_B for each of the two Ti atoms first neighbors of the V_O.

APPENDIX B: SBH CALCULATIONS

Different methods can be used to calculate the SBH (by aligning the core levels or calculating the averaged electrostatic potential for example); these methods give in general very close results [22], which we verified for the perfect interfaces. In the present study we preferred to use the LDOS to calculate the *p*-type SBH: to do so, we made the energy difference between the Fermi level which is set up by the Fe layer and the different gap states near the interface and the VBM at the center of the STO film. Considering that our STO layer has a sufficient thickness, the DOS at the center should be aligned to those of the bulk; otherwise some corrections would be necessary. As we can see from Fig. 4(b), the variation of the 1*s* core level energy of the oxygen atom at the center of the slab corresponds almost exactly to the calculated *p*-SBH, which indicates that such correction is negligible and our slab sufficiently thick. When including an oxygen vacancy, we verified that the band-gap width at the center of the slab almost does not vary compared to the bulk value, allowing us to use the LDOS to calculate the SBH.

If the bands from the Fe and STO layers are well aligned, the *p*-SBH can be correctly calculated. The *n*-SBH can then be obtained either by doing the difference between the Fermi level and the CBM at the center of the STO layer, if the STO gap is well calculated, or by doing the difference between the experimental band gap (3.2 eV) and the *p*-SBH. By considering the experimental band gap, the *n*-SBH is then approximately 0.4 eV higher than with the direct calculation with $U_{\text{eff}} = 8$ eV.

Still if $U_{\text{eff}} = 8$ eV, we found a preservation of the Schottky regime for most of the systems and we calculated the *n*- and *p*-SBH. It is difficult to choose a correct value for the U_{eff} parameter and compromises have to be made between a correct description of the vacancy electronic states and a sufficiently high value of the band gap near the Fermi level, this, by keeping in mind the limited size of our slab and the high vacancy content of our supercell. We chose to mostly focus on an artificially high value of U_{eff} as proposed in Ref. [23] in order to give a general trend about the variation of the calculated SBH and to be consistent with the nonzero SBH measured by Catrou *et al.* for the same interface [8]. As mentioned previously, with this approximation, we calculated an ionization potential of 5.40 and 3.78 eV, respectively, for a TiO_2- and a SrO-terminated STO surfaces, which is close (even if lower) to the values of 6.71 and 4.41 eV, calculated by Stevanović *et al.* [73], who have used a combination of *GW* and DFT + *U* methods. Experimental values have been reported to be in the range of 7.2–7.9 eV and may vary as a function of the oxygen adsorption/desorption: a larger ionization potential is measured for oxygen-rich conditions [74–76].

As a lower value of U_{eff} is often used in the literature, we also provide the calculated SBH for $U_{\text{eff}} = 0$ or 4 eV in Table II. For these lower U_{eff}, the SBH can only be calculated if the V_O is located in the TiO_2 interface atomic layer; when it is located deeper in the film, the system is in an ohmic regime and the Fermi level crosses the conduction band of STO.

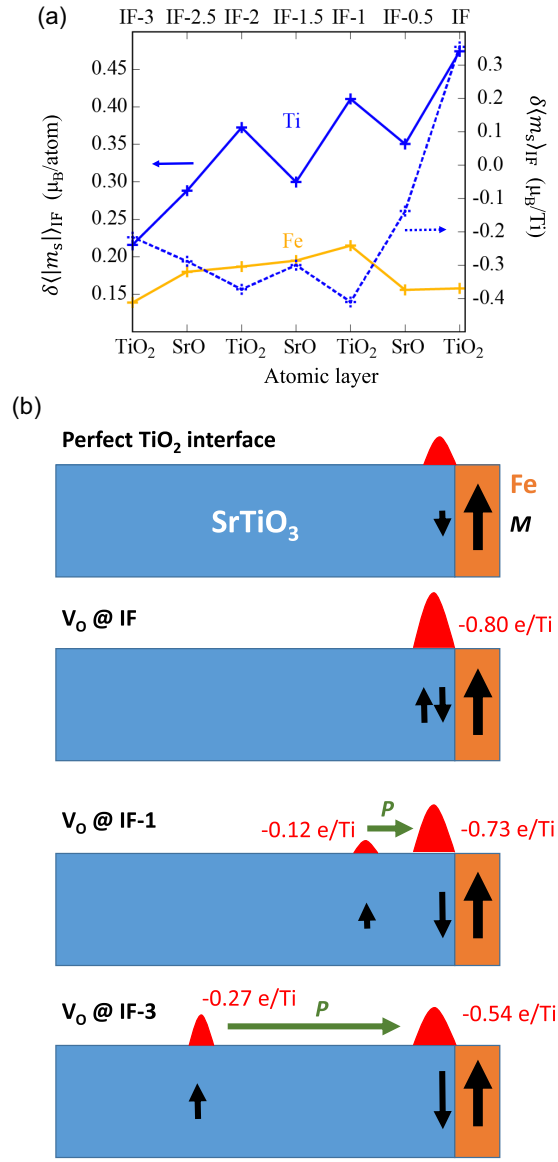

FIG. 10. (a) Variation of the averaged spin magnetic moment $\langle m_s \rangle$ (dotted line, right) and its absolute value $\langle |m_s| \rangle$ (solid line, left) of the interfacial Ti and Fe atoms as a function of the position of the oxygen vacancy near the TiO_2-terminated interface. The values are given relatively to the moment of the same atoms at the perfect interface. (b) Schematic representation of the charge localization (in red), leading to the emergence of an electric polarization *P* (green arrow) and of the magnetic ordering (black arrows) as a function of the V_O position.

APPENDIX C: MAGNETIC PROPERTIES OF THE OXYGEN-DEFICIENT TiO_2-TERMINATED INTERFACES

Figure 10(a) shows both the variation of the spin magnetic moment m_s of the Ti and Fe atom at the TiO_2-terminated interface and of its absolute value when a V_O is introduced near the Fe/STO interface. The deviation is given according to the spin magnetic moment of the Ti or Fe atoms at the perfect interface (respectively −0.322 and 2.31 μ_B). Thanks to this figure we will describe in detail how the charge reconstruction resulting from the presence of the V_O affects the magnetic

properties of the interface and we will derive a scenario which is summarized by Fig. 10(b). The description of the magnetic properties changes was beyond the scope of our paper, mostly focused on the formation of SBH, but it remains very close due to its link with the electronic structure. It may also be of interest to understand the effect the V_O's have on the magnetoelectric properties of such an interface.

First, considering the absolute-value variation of the spin magnetic moments of the Ti atoms (solid blue curve) gives approximated information about the charges transferred to the interface. When the V_O is in the TiO_2 interface layer, we expect the MIGSs to be populated by the two electrons released by the neutral vacancy (i.e., 0.5 electron/Ti atom), which corresponds to the calculated increase of $\delta\langle|m_s|\rangle_{IF}$ by 0.475 μ_B. When the V_O is located in atomic layers further from the interface, only a part of the released charges stays localized in the TiO_2 layer first neighbor of the vacancy, the other part being transferred to the TiO_2 interface layer. The further the V_O is from the interface, the lower the amount of transferred charges; which is consistent with the decrease of the averaged absolute value of the spin magnetic moment of the interfacial Ti atoms from 0.475 μ_B (for the V_O at IF) to 0.22 μ_B (for the V_O at IF-3). Concerning the charges which are localized near the V_O, as their amount increases when the V_O is moved toward the center of the slab, we observe subsequently an increase of the induced spin magnetic moment on the first-neighbor Ti atoms, which reaches the value of -0.53 μ_B for the two Ti atoms first neighbor of the V_O and located in the TiO_2(IF-3) layer. When the V_O is in a SrO layer, only the first-neighbor Ti atom in the adjacent TiO_2 layer away from the interface possesses a non-null induced magnetic moment of approximately -0.5 μ_B, while the other Ti atom first neighbor of the vacancy has a 0 μ_B spin magnetic moment. The aforementioned results stays qualitatively correct for a lower value of U_{eff} parameter (4 eV), even if quantitatively the magnetic moment induced by the localized charge on the Ti atoms first neighbor of the V_O is decreased by a factor 2 (when the V_O is at IF-3); in agreement with the bulk calculations described in Appendix A, the lower the value of U_{eff}, the more the charges will populate the CBM of STO, constituted of (d_{xy}, d_{xz}, d_{yz}) bands instead of the localized $d_{x^2-y^2}$ or d_{z^2} states. Still by comparing these results with the bulk calculations, the band bending induced by the interface adds a space separation of these two sets of occupied d bands and favors the occupation of the (d_{xy}, d_{xz}, d_{yz}) bands near the interface.

If we analyze now the variation of the spin magnetic moment of the interfacial Ti atoms (dotted blue curve), which results from the charge transfer, we can have additional information concerning some possible changes in the magnetic coupling between Ti atoms. It is for example possible to see that we have a change of its sign when the V_O is moved away from the IF (between IF and IF-0.5). When the V_O is located in the TiO_2 interfacial layer, the spin magnetic moments on the Ti atoms are of $+0.83$ and -0.76 μ_B, corresponding to an almost compensated in-plane antiferromagnetic ordering and leading to a nearly 0 μ_B value on average. When the V_O is moved in the IF-0.5 SrO layer, then only the Ti atom first neighbor of the V_O will have the sign of its magnetic moment reversed (to a positive value), the other Ti atoms keeping a negative magnetic moment. In consequences, $\delta\langle m_s\rangle_{IF}$ will decrease. Moving again the V_O further from the interface, the Ti atoms will feel less the effect of the V_O and they will remain all ferromagnetically coupled, with negative spin magnetic moments and a larger absolute value than the perfect interface ($+0.22$ μ_B when the V_O is in the IF-3 layer). From the point where the V_O is located in the TiO_2(IF-1) layer, $\delta\langle m_s\rangle_{IF}$ will then increase linearly due to the lowering of the transferred charge to the interface.

Finally, compared with the perfect TiO_2-terminated interface, the interfacial Fe spin magnetic moments (yellow curve) also undergo some slight variations as a function of the position of the oxygen vacancy. They increase from 2.31 to 2.47 μ_B, when an oxygen vacancy is located at the interface (IF layer). The variation of the Fe magnetic moment at the interface as a function of the V_O location is less than 0.05 μ_B for the calculated positions; it has a maximum of $+0.22$ μ_B when the V_O is in the TiO_2(IF-1) layer, i.e., when the Ti-atom magnetic moments reach also a maximum (maximum of transferred charge with a ferromagnetic coupling), and it decreases toward 0 μ_B (i.e., the bulk value), when the V_O is moved toward the center of the slab.

[1] M. Jang, Nano Converg. **3**, 11 (2016).
[2] N. A. Al-Ahmadi, Mater. Res. Express **7**, 032001 (2020).
[3] M. W. Allen and S. M. Durbin, Appl. Phys. Lett. **92**, 122110 (2008).
[4] T. Berthold, J. Rombach, T. Stauden, V. Polyakov, V. Cimalla, S. Krischok, O. Bierwagen, and M. Himmerlich, J. Appl. Phys. **120**, 245301 (2016).
[5] S. Müller, H. von Wenckstern, F. Schmidt, D. Splith, H. Frenzel, and M. Grundmann, Semicond. Sci. Technol. **32**, 065013 (2017).
[6] T. Schultz, S. Vogt, P. Schlupp, H. von Wenckstern, N. Koch, and M. Grundmann, Phys. Rev. Applied **9**, 064001 (2018).
[7] H. Stöcker, M. Zschornak, J. Seibt, F. Hanzig, S. Wintz, B. Abendroth, J. Kortus, and D. C. Meyer, Appl. Phys. A **100**, 437 (2010).
[8] P. Catrou, S. Tricot, G. Delhaye, J.-C. Le Breton, P. Turban, B. Lépine, and P. Schieffer, Phys. Rev. B **98**, 115402 (2018).
[9] F. Gunkel, D. V. Christensen, Y. Z. Chen, and N. Pryds, Appl. Phys. Lett. **116**, 120505 (2020).
[10] A. Ohtomo and H. Y. Hwang, Nature (London) **427**, 423 (2004).
[11] A. F. Santander-Syro, O. Copie, T. Kondo, F. Fortuna, S. Pailhès, R. Weht, X. G. Qiu, F. Bertran, A. Nicolaou, A. Taleb-Ibrahimi, P. Le Fèvre, G. Herranz, M. Bibes, N. Reyren, Y. Apertet, P. Lecoeur, A. Barthélémy, and M. J. Rozenberg, Nature (London) **469**, 189 (2011).
[12] T. C. Rödel, F. Fortuna, S. Sengupta, E. Frantzeskakis, P. L. Fèvre, F. Bertran, B. Mercey, S. Matzen, G. Agnus, T. Maroutian, P. Lecoeur, and A. F. Santander-Syro, Adv. Mater. **28**, 1976 (2016).

[13] A. Kalabukhov, R. Gunnarsson, J. Börjesson, E. Olsson, T. Claeson, and D. Winkler, Phys. Rev. B **75**, 121404 (2007).

[14] W. Siemons, G. Koster, H. Yamamoto, W. A. Harrison, G. Lucovsky, T. H. Geballe, D. H. A. Blank, and M. R. Beasley, Phys. Rev. Lett. **98**, 196802 (2007).

[15] W. Meevasana, P. D. C. King, R. H. He, S.-K. Mo, M. Hashimoto, A. Tamai, P. Songsiriritthigul, F. Baumberger, and Z.-X. Shen, Nat. Mater. **10**, 114 (2011).

[16] K. Szot, W. Speier, G. Bihlmayer, and R. Waser, Nat. Mater. **5**, 312 (2006).

[17] M. Janousch, G. Meijer, U. Staub, B. Delley, S. Karg, and B. Andreasson, Adv. Mater. **19**, 2232 (2007).

[18] R. Muenstermann, T. Menke, R. Dittmann, S. Mi, C.-L. Jia, D. Park, and J. Mayer, J. Appl. Phys. **108**, 124504 (2010).

[19] R. T. Tung, Appl. Phys. Rev. **1**, 011304 (2014).

[20] N. F. Mott, Proc. R. Soc. London Ser. A **171**, 27 (1939).

[21] W. Schottky, Z. Phys. **113**, 367 (1939).

[22] M. Mrovec, J.-M. Albina, B. Meyer, and C. Elsässer, Phys. Rev. B **79**, 245121 (2009).

[23] J. Lee, C. Lin, and A. A. Demkov, Phys. Rev. B **87**, 165103 (2013).

[24] X. Ma, Y. Dai, M. Li, and B. Huang, Phys. Chem. Chem. Phys. **19**, 774 (2017).

[25] D. Ricci, G. Bano, G. Pacchioni, and F. Illas, Phys. Rev. B **68**, 224105 (2003).

[26] J. P. Buban, H. Iddir, and S. Öğüt, Phys. Rev. B **69**, 180102 (2004).

[27] M.-Q. Cai, Y.-J. Zhang, G.-W. Yang, Z. Yin, M.-S. Zhang, W.-Y. Hu, and Y.-G. Wang, J. Chem. Phys. **124**, 174701 (2006).

[28] J. Carrasco, F. Illas, N. Lopez, E. A. Kotomin, Y. F. Zhukovskii, R. A. Evarestov, Y. A. Mastrikov, S. Piskunov, and J. Maier, Phys. Rev. B **73**, 064106 (2006).

[29] D. D. Cuong, B. Lee, K. M. Choi, H.-S. Ahn, S. Han, and J. Lee, Phys. Rev. Lett. **98**, 115503 (2007).

[30] V. E. Alexandrov, E. A. Kotomin, J. Maier, and R. A. Evarestov, Eur. Phys. J. B **72**, 53 (2009).

[31] Y. Zhukovskii, E. Kotomin, S. Piskunov, and D. Ellis, Solid State Commun. **149**, 1359 (2009).

[32] Z. Hou and K. Terakura, J. Phys. Soc. Jpn. **79**, 114704 (2010).

[33] E. A. Kotomin, V. Alexandrov, D. Gryaznov, R. A. Evarestov, and J. Maier, Phys. Chem. Chem. Phys. **13**, 923 (2011).

[34] C. Mitra, C. Lin, J. Robertson, and A. A. Demkov, Phys. Rev. B **86**, 155105 (2012).

[35] M. Choi, F. Oba, Y. Kumagai, and I. Tanaka, Adv. Mater. **25**, 86 (2013).

[36] A. R. Silva and G. M. Dalpian, J. Appl. Phys. **115**, 033710 (2014).

[37] W. Sitaputra, N. Sivadas, M. Skowronski, D. Xiao, and R. M. Feenstra, Phys. Rev. B **91**, 205408 (2015).

[38] J. J. Brown, Z. Ke, W. Geng, and A. J. Page, J. Phys. Chem. C **122**, 14590 (2018).

[39] H. O. Jeschke, J. Shen, and R. Valentí, New J. Phys. **17**, 023034 (2015).

[40] G. Kresse and J. Hafner, Phys. Rev. B **49**, 14251 (1994).

[41] G. Kresse and J. Furthmüller, Phys. Rev. B **54**, 11169 (1996).

[42] P. E. Blöchl, Phys. Rev. B **50**, 17953 (1994).

[43] G. I. Csonka, J. P. Perdew, A. Ruzsinszky, P. H. T. Philipsen, S. Lebègue, J. Paier, O. A. Vydrov, and J. G. Ángyán, Phys. Rev. B **79**, 155107 (2009).

[44] S. L. Dudarev, G. A. Botton, S. Y. Savrasov, C. J. Humphreys, and A. P. Sutton, Phys. Rev. B **57**, 1505 (1998).

[45] T. Ochs, S. Köstlmeier, and C. Elsässer, Integrated Ferroelect. **32**, 267 (2001).

[46] I. I. Oleinik, E. Y. Tsymbal, and D. G. Pettifor, Phys. Rev. B **65**, 020401 (2001).

[47] A. Asthagiri and D. S. Sholl, J. Chem. Phys. **116**, 9914 (2002).

[48] H. J. Monkhorst and J. D. Pack, Phys. Rev. B **13**, 5188 (1976).

[49] M. Peressi, N. Binggeli, and A. Baldereschi, J. Phys. D: Appl. Phys. **31**, 1273 (1998).

[50] M. Stengel, P. Aguado-Puente, N. A. Spaldin, and J. Junquera, Phys. Rev. B **83**, 235112 (2011).

[51] D. Li, C. Barreteau, and A. Smogunov, Phys. Rev. B **93**, 144405 (2016).

[52] C.-G. Duan, S. S. Jaswal, and E. Y. Tsymbal, Phys. Rev. Lett. **97**, 047201 (2006).

[53] M. Fechner, I. V. Maznichenko, S. Ostanin, A. Ernst, J. Henk, P. Bruno, and I. Mertig, Phys. Rev. B **78**, 212406 (2008).

[54] R. Arras and S. Cherifi-Hertel, ACS Appl. Mater. Interfaces **11**, 34399 (2019).

[55] R. F. W. Bader, *Atoms in Molecules: A Quantum Theory* (Oxford University Press, New York, 1990).

[56] E. Sanville, S. D. Kenny, R. Smith, and H. G., J. Comput. Chem. **28**, 899 (2007).

[57] W. Tang, E. Sanville, and G. Henkelman, J. Phys.: Condens. Matter **21**, 084204 (2009).

[58] C. G. Van de Walle and A. Janotti, Phys. Status Solidi B **248**, 19 (2011).

[59] C. Freysoldt, B. Grabowski, T. Hickel, J. Neugebauer, G. Kresse, A. Janotti, and C. G. Van de Walle, Rev. Mod. Phys. **86**, 253 (2014).

[60] T. Tamura, S. Ishibashi, K. Terakura, and H. Weng, Phys. Rev. B **80**, 195302 (2009).

[61] L. Yu and A. Zunger, Nat. Commun. **5**, 5118 (2014).

[62] D. C. Vaz, E. Lesne, A. Sander, H. Naganuma, E. Jacquet, J. Santamaria, A. Barthélémy, and M. Bibes, Adv. Mater. **29**, 1700486 (2017).

[63] *CRC Handbook of Chemistry and Physics*, internet version (CRC, Boca Raton, FL, 2005), pp. 12–124.

[64] K. Uchida, S. Tsuneyuki, and T. Schimizu, Phys. Rev. B **68**, 174107 (2003).

[65] T. Ikeda, T. Kobayashi, M. Takata, T. Takayama, and M. Sakata, Solid State Ionics **108**, 151 (1998).

[66] W. Zhong and D. Vanderbilt, Phys. Rev. Lett. **74**, 2587 (1995).

[67] E. Bousquet, M. Dawber, N. Stucki, C. Lichtensteiger, P. Hermet, S. Gariglio, J.-M. Triscone, and P. Ghosez, Nature (London) **452**, 732 (2008).

[68] C.-H. Lin, C.-M. Huang, and G. Y. Guo, J. Appl. Phys. **100**, 084104 (2006).

[69] A. Vasudevarao, A. Kumar, L. Tian, J. H. Haeni, Y. L. Li, C.-J. Eklund, Q. X. Jia, R. Uecker, P. Reiche, K. M. Rabe, L. Q. Chen, D. G. Schlom, and V. Gopalan, Phys. Rev. Lett. **97**, 257602 (2006).

[70] C. Lin and A. A. Demkov, Phys. Rev. Lett. **111**, 217601 (2013).

[71] M. Altmeyer, H. O. Jeschke, O. Hijano-Cubelos, C. Martins, F. Lechermann, K. Koepernik, A. F. Santander-Syro, M. J.

Rozenberg, R. Valentí, and M. Gabay, Phys. Rev. Lett. **116**, 157203 (2016).

[72] S. Okamoto, A. J. Millis, and N. A. Spaldin, Phys. Rev. Lett. **97**, 056802 (2006).

[73] V. Stevanović, S. Lany, D. S. Ginley, W. Tumas, and A. Zunger, Phys. Chem. Chem. Phys. **16**, 3706 (2014).

[74] V. E. Henrich, G. Dresselhaus, and H. J. Zeiger, Phys. Rev. B **17**, 4908 (1978).

[75] J. Robertson and C. W. Chen, Appl. Phys. Lett. **74**, 1168 (1999).

[76] R. Schafranek and A. Klein, Solid State Ionics **177**, 1659 (2006).